Quantitative Analysis of Cerebrospinal Fluid Flow in Complex Regions by Using Phase Contrast Magnetic Resonance Imaging

Natalia Flórez,[1] Roger Bouzerar,[2] David Moratal,[3,4] Marc-Etienne Meyer,[2] Luis Martí-Bonmatí,[1] Olivier Balédent[2]

[1] Department of Radiology, Hospital Quirón, Valencia, Spain

[2] Department of Imaging and Biophysics, University Hospital, Amiens, France

[3] Center for Biomaterials and Tissue Engineering, Universitat Politècnica de València, València, Spain

[4] Department of Electronic Engineering, Universitat Politècnica de València, València, Spain

Received 28 May 2010; accepted 27 April 2011

ABSTRACT: To develop a method for segmenting cerebrospinal fluid (CSF) regions with complex, inhomogeneous pulsatile patterns in phase contrast magnetic resonance imaging (PC-MRI) sequences. Our approach used various temporal features of flow behavior as input attributes in an unsupervised k-means classification algorithm. CSF flow parameters for the cervical subarachnoid spaces and the pontine cistern were calculated in 26 healthy volunteers. Background and aliasing corrections were applied automatically. The algorithm's reproducibility was determined by calculating two parameters (area and stroke volume) while varying the initially selected seed point. The influence of background correction on these parameters was also assessed. The method was highly reproducible, with coefficients of variation of 3 and 4% for the cervical stroke volume and area, respectively. In an analysis of variance, background correction did not have a statistically significant effect on either the stroke volume ($p = 0.32$) or the CSF net mean flow ($p = 0.69$) at the C2C3 level. The method presented here enables rapid, reproducible, quantitative analysis of CSF flow in complex regions such as the C2C3 subarachnoid spaces and the pontine cistern. Int J Imaging Syst Technol, 21, 290–297, 2011; Published online in Wiley Online Library (wileyonlinelibrary.com). DOI 10.1002/ima.20294

Key words: CSF flow; PC-MRI; k-means; segmentation; pontine cistern

I. INTRODUCTION

The brain is probably the most complex structure in the human body. With a view to understanding neurological disorders such as hydrocephalus, the brain's motion and the distribution of cerebrospinal fluid (CSF) pulsations within the craniospinal axis in response to rhythmic cerebral blood volume variations during the cardiac cycle have been extensively investigated (Enzmann and Pelc, 1991; Enzmann and Pelc, 1992; Bradley, 1992; Alperin et al., 1996; Henry-Feugeas et al., 2000; Egnor et al; 2002).

The combination of phase contrast magnetic resonance imaging (PC-MRI) and peripheral cardiac gating has enabled the precise, noninvasive, quantitative analysis of CSF and blood flow variations during the cardiac cycle (Thomsen et al., 1990; Nitz et al., 1992; Greitz et al., 1993; Henry-Feugeas et al., 1993; Greitz, 1993; Enzmann and Pelc, 1993; Bhadelia et al., 1995; Kim et al., 1999). This technique has facilitated the study of the central nervous system's pulsation at several intracranial and extracranial locations (Alperin et al., 1996; Bhadelia et al., 1997; Miyati et al., 2003; Baledent et al., 2004; Wagshul et al., 2006). The analysis of blood and CSF flow dynamics within the brain enables the calculation of periodical, intracranial volume changes, and the simulation and assessment of intracranial compliance and pressure (Alperin, 2004; Baledent et al., 2006; Miyati et al., 2007). Several authors have proposed CSF flow parameters for use in the diagnosis of hydrocephalus and the prediction of shunt responses (Bradley et al., 1996; Luetmer et al., 2002).

Nevertheless, the reproducibility and reliability of flow quantization using PC-MRI depend greatly on the postprocessing method used to accurately delineate the region of interest (ROI) (Wolf et al., 1993; Pelc, 1995). The first studies of automatic or semi-automatic segmentation methods using PC-MRI images were applied to blood vessels (Kozerke et al., 1999; Yuan et al., 1999; Box et al., 2003). To study neurological and cerebrovascular diseases, the

Grant sponsor: Generalitat Valenciana; *Grant number:* CTBPRB/2004/342 FPI.
Correspondence to: Olivier Balédent; e-mail: olivier.baledent@chu-amiens.fr

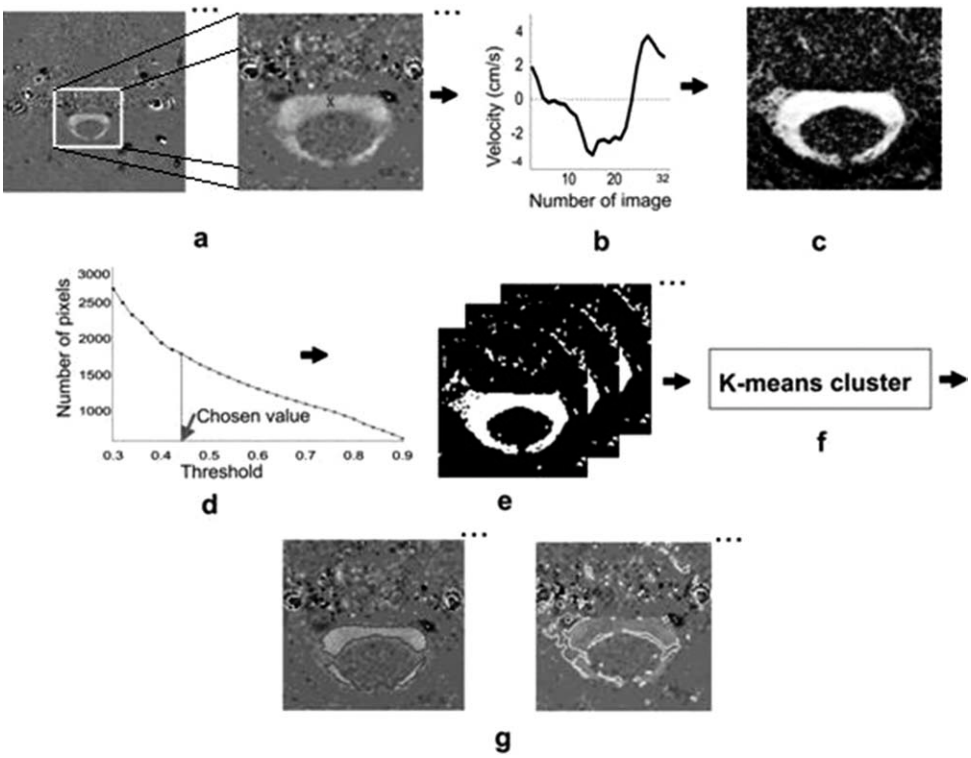

Figure 1. CSF segmentation algorithm applied to the C2C3 subarachnoid spaces. (a) ROI defined following selection of an initial seed point inside the CSF spaces to be investigated. (b) By starting from the selected point ("x"), a reference velocity profile is obtained and a correlation map is created (c). (d) A curve representing the number of segmented pixels above the threshold values (ranging from 0.3 to 0.9) is obtained from the correlation map; the slopes between two consecutive points on the curve are calculated and the threshold is set to the first slope value below the average slope. (e) The threshold value is applied to the correlation map and the resulting mask is multiplied by the sequence of images. After the implementation of k-means clustering (f), the resulting two classes correspond to pixels with CSF flow and pixels containing blood flow or background tissue. The contours on the bottom left and bottom right images delineate the automatically selected ROI and the discarded regions, respectively (g).

exploration of CSF flows in anatomically complex regions requires advanced segmentation methods. Baledent et al. (2001) developed a method (based upon fast Fourier transform of the time velocity series) to segment both vessels and CSF spaces. They used the fundamental frequency amplitude of pixel velocity variations during the cardiac cycle to identify oscillatory CSF and blood flows. Alperin and Lee (2003) subsequently used both temporal and spatial information for lumen boundary identification and developed a cross-correlation unbiased threshold method to improve reproducibility in the segmentation of CSF spaces and vessels.

CSF motion inside the pontine cistern is a reflection of CSF oscillations outside of ventricles and should be altered in case of cerebral haemorrhage leading to hydrocephalus. Owing to its geometrical shape, this complex area is not easy to segment. In addition, high velocity pixels representing the basilar trunk are embedded inside the low velocity pixels representing the cistern so that this can lead to critical segmentation issues.

The aim of this work was firstly to develop an approach for analyzing CSF flow dynamics in anatomically complex regions like the cervical subarachnoid spaces and the pontine cistern and secondly to evaluate the impact of background correction in phase contrast imaging.

The method presented here was inspired by the pulsatility-based segmentation algorithm presented from Alperin and Lee (2003), and the process was completed by the inclusion of a segmentation algorithm based on observations of CSF physiological behavior (Baledent et al., 2001).

II. MATERIAL AND METHODS

A. Subjects and Image Acquisition. Twenty-six healthy volunteers (10 women and 16 men; mean age: 29 $\pm$ 4 years; age range: 22–44) were included in the study. CSF flows at the C2C3 level were analysed in all 26 subjects, whereas CSF flows in the pontine cistern were studied in a subset of 16 subjects (six women and 10 men).

The volunteers were explored using a 3T MR scanner (Signa HDx, General Electric Healthcare, Milwaukee, WI). The subjects were lying supine with the neck in a neutral position. CSF flow acquisition scans were perpendicular to the flow direction.

Velocity images were acquired using retrospectively gated cine phase-contrast pulse sequences with the following parameters: TR = 12 ms, TE = 7 ms, FOV = 14 $\times$ 14 cm, matrix size = 256 $\times$ 256, slice thickness = 5 mm, flip angle = 30°, NEX = 1, VPS = 4. The velocity-encoding (V_{enc}) parameter was set to 5 cm/s for both regions.

Each series of reconstructed data consisted of 32 phase images, which were equally distributed throughout the cardiac cycle and were associated with the corresponding magnitude images. The acquisition time was about 2 min per level, depending on the subject's heart rate.

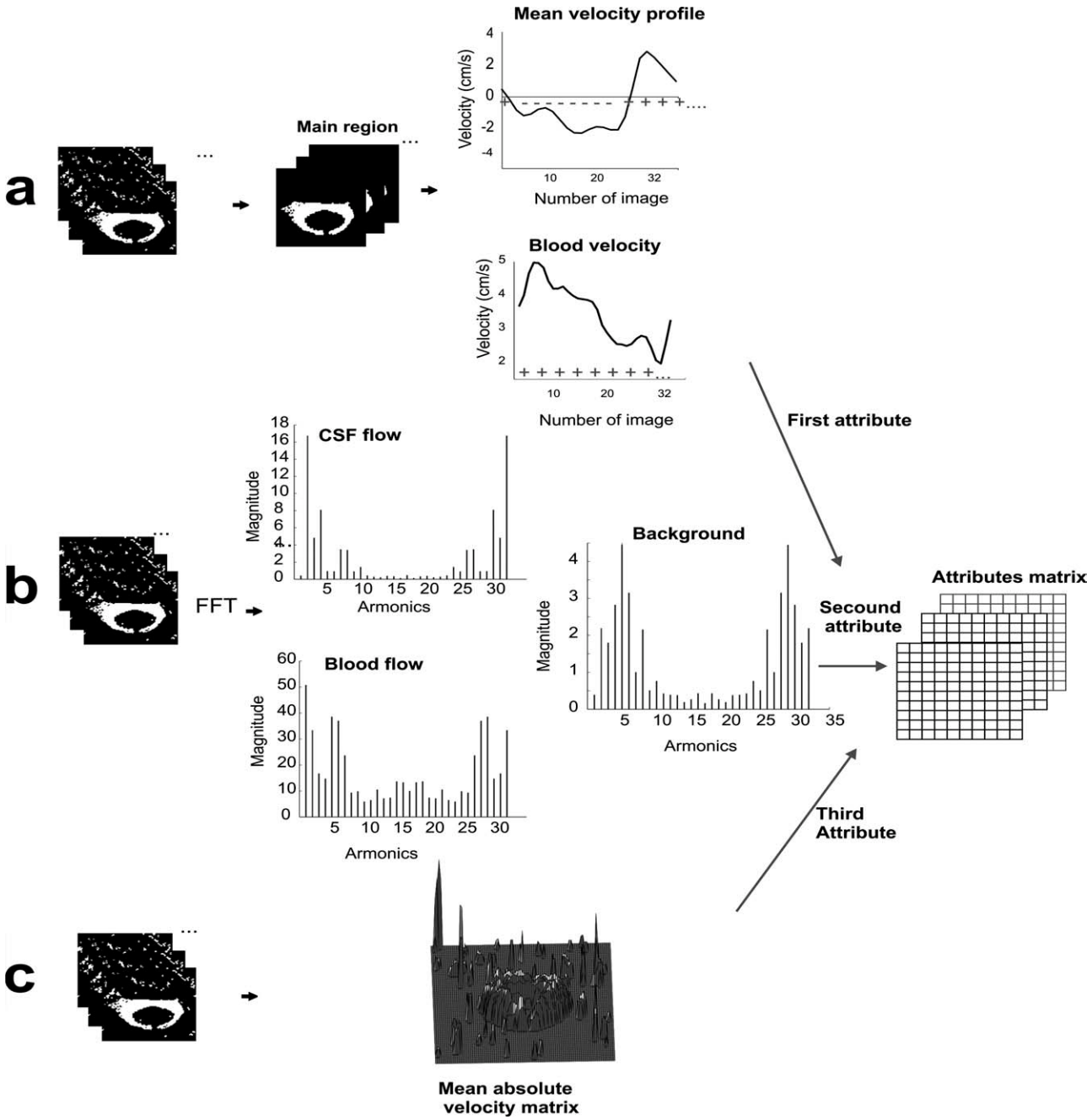

Figure 2. Attributes used in the k-means clustering step. The first attribute is the total number of sign agreements obtained when comparing the averaged curve and the pixel velocity profile. The second attribute is the magnitude of the fundamental frequency component, which corresponds to the subject's heart rate. The third attribute is defined as the mean absolute velocity value (calculated from the phase image sequence in each pixel).

B. Automatic CSF Flow Segmentation. The method developed in this paper was implemented using MATLAB (The MathWorks, Natick, MA). The process was manually initialized by selecting a point within a high-contrast phase image of the CSF ROI. A rectangular window around this point was created (Fig. 1a).

Using the selected point, a reference velocity waveform (Fig. 1b) was defined to compute the correlation map (Alperin and Lee, 2003) (Fig. 1c). The next step consisted in reproducibly and automatically determining a cross-correlation threshold value, to extract CSF pixels. To this end, the curve representing the number of segmented pixels was computed as a function of threshold values ranging from 0.3 to 0.9 in steps of 0.02, as suggested by Alperin and Lee (2003). However, in our method, the mean slope values between consecutive points on the curve were calculated to choose the best threshold value for CSF segmentation. The threshold was set to the first slope value below the calculated mean slope (Fig. 1d). Hence, the threshold value was automatically selected in a reproducible way for each

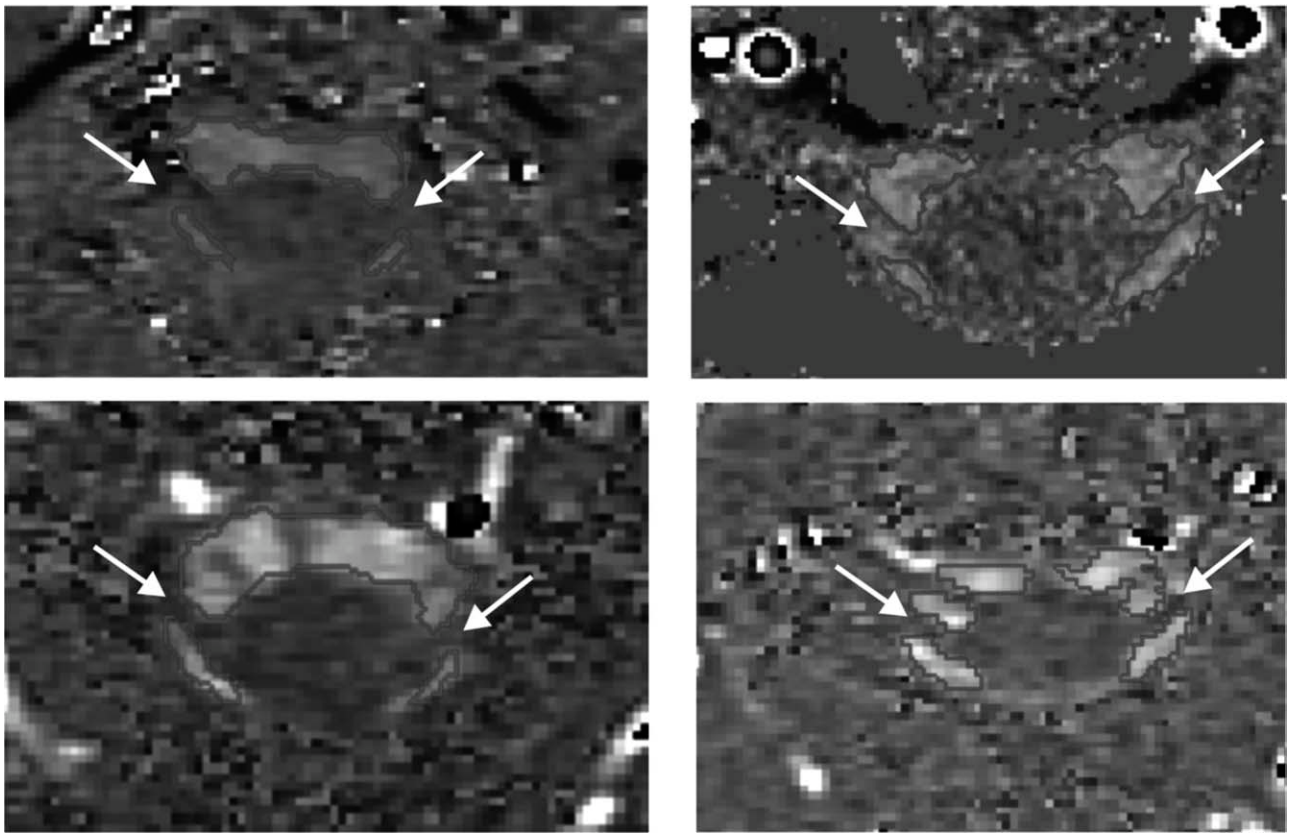

Figure 3. ROIs at the C2C3 level where CSF flow area is divided into compartments. The spinal nerves (arrows) in the image slices are removed from the segmentation.

segmentation procedure, to improve the method's robustness and obtain a CSF segmentation mask (Fig. 1e).

To clearly delineate the ROI, we added a final k-means clustering step to Alperin's method (MacQueen, 1967) (Fig. 1f).

The k-means cluster was defined with $k = 2$ classes, corresponding to the two types of pixel encountered in the matrix: the first class contains pixels with CSF flow behavior, whereas the second contains pixels with blood flow or background tissue behaviors. Initially, the position of the cluster centroids was randomly selected, and the squared Euclidean distance between each object and the centroids was calculated.

Classification using cluster analysis is based on a fixed number of attributes per pixel. Based on physiological CSF oscillations, we included three attributes that temporally characterize the flow behavior (Fig. 2). The first attribute relates to the coherence of the flow direction for all considered pixels. To determine this first attribute, the region with the highest area was used and CSF pixels' temporal velocity curves within this region were averaged. Hence, the first attribute of each pixel corresponded to the number of sign agreements when comparing the averaged curve and the pixel velocity profile (Fig. 2a). A positive sign represented a velocity value greater than 0, whereas a negative sign represented a velocity value below 0. The amplitudes were not compared. It was thus possible to discard aliasing flows (i.e., blood flows).

The second attribute was the magnitude of the signal's fundamental frequency component, corresponding to the subject's heart rate. This component, used to determine pulsatile regions (Baledent et al., 2001) and remove background noise, was calculated using a fast Fourier transform of the 32 velocity values spanning the cardiac cycle in each pixel (Baledent et al., 2001) (Fig. 2b). The third and last attribute was defined as the mean absolute velocity value calculated from the phase image sequence in each pixel. Thus, the intermediate velocities of CSF flows were distinguished from higher velocities in blood areas, lower velocities in nonpulsatile regions and background noise (Fig. 2c).

Once these attributes had been calculated, a k-means cluster analysis was performed. The class that contained the highest number of pixels was automatically chosen as the representation of the ROI (Fig. 1g). The combination of these attributes excludes partial volume effects near the ROI's borders and facilitates the extraction of the spinal nerves that divide the cervical CSF region into compartments (Fig. 3). The segmentation process (the results of which are shown in Fig. 1) takes about 1 min on a computer with a 1.6-GHz Intel Pentium processor and 1 GB of RAM.

C. Data Correction. A background correction was applied to compensate for the systematic errors caused by imperfect removal of eddy currents from the phase values. The correction factor was calculated as the mean offset per frame in background baseline regions, to subtract this value from the apparent velocities in the ROI. After the operator had selected a point in the midbrain, a circular, 42 mm^2 ROI was automatically built around it. Another automatic correction was applied to the aliased pixels in the ROI (Baledent et al., 2001).

Figure 4. Ten different initial seed points set to evaluate the reproducibility of the CSF segmentation algorithm. This process was performed in five different subjects.

D. Data analysis. Five flow parameters were calculated for the C2C3 level and the pontine cistern: the net mean flow (ml/min), defined as the algebraic sum of the mean flow over the 32 cardiac phases; the stroke volume (µl/cycle), calculated as the mean volume of fluid moving craniocaudally during systole and in the opposite direction during diastole; the minimum and maximum peak velocities (mm/s) and the ratio of the stroke volume in the pontine cistern to that in the C2C3 subarachnoid space.

E. Reproducibility and Statistical Analysis. The reproducibility of the newly developed CSF segmentation algorithm was determined by varying the initially selected seed point. One observer initiated the segmentation of the cervical CSF images 10 times in five subjects and noted the mean stroke volume and area values in each case (Fig. 4).

The variability of the obtained measurements was assessed by calculating the coefficient of variation (CV: the ratio of standard deviation in each group of measurements to the mean value for the group).

An analysis of variance (ANOVA) was used to investigate the similarity of the values obtained for the C2C3 region in the presence and absence of background correction. Null hypothesis were verified using a two-tailed test. The threshold for statistical significance was set to $p = 0.05$.

III. RESULTS

A. Reproducibility. The mean CV values obtained for the cervical CSF area and the mean stroke volume in healthy subjects showed that the new method's reproducibility is not affected by the initially selected seed point. Mean CVs of $3 \pm 1.5\%$ and $4 \pm 2.4\%$ were obtained for the mean stroke volume and the area, respectively. All the CV values were below 5%.

B. Data Corrections. A one-way ANOVA revealed the lack of statistically significant differences for both the mean stroke volume ($p = 0.32$) and the net mean CSF flow ($p = 0.69$) calculated with and without background correction. The means and standard deviations are summarized in Table I.

Aliased pixels were detected and corrected in two subjects for cervical CSF flow and in three subjects for pontine cistern CSF flow.

C. Flow Amplitude Measurements. Mean stroke volumes, net mean flows, maximum and minimum peak velocities and areas calculated for the C2C3 spaces and the pontine cistern are shown in Table II. The stroke volume ratio for the pontine cistern and the C2C3 subarachnoid space was $48 \pm 28\%$ (range: 16–90%).

IV. DISCUSSION

Our approach enables the delineation of CSF regions with complex, inhomogeneous pulsatile patterns. Depending on the slice position, the cervical CSF flow area is not a single ROI, as spinal nerves can divide it in several compartments (namely the posterior, anterior and lateral subarachnoid spaces, as shown in Fig. 3). Each compartment has its own CSF flow pattern with a significant time shift (Henry-Feugeas et al., 2000). By taking this morphological characteristic into account, the algorithm presented here provides accurate CSF segmentation.

The need of reproducibility and reliability of MRI flow images by postprocessing prompted us to develop a semi-automatic method that uses various temporal features of flow behavior as input attributes in an unsupervised k-means classification algorithm. Segmentation techniques based on temporal information from flow waveforms help ROI delineation.

The effectiveness of the k-means clustering implemented in this work is probably due to the fact that attributes such as the absolute velocity flow value and the fundamental frequency magnitude enable one to clearly distinguish pulsatile flow regions from background tissues and noise.

The main advantages of the method presented herein are fast, consistent, operator-independent ROI delineation. In addition, physiological behavior of CSF flows are taken into account. Nevertheless, as other segmentation algorithms, the main problem remains the selection of the threshold ''cut off'' value. Figure 5 shows the clustered pixels after applying the threshold values ranging from 0.3 to 0.9 in steps of 0.02; the threshold value of 0.4 calculated

Table I. Mean value, standard deviation and significance values of one-way Anova test for the measurements obtained with or without background correction at C2C3 level.

Parameters		*n*	Mean (SD)	Range [Min, Max]	*p*
Mean stroke volume (µl/cycle)	Background correction	26	383 (133)	[198, 697]	0.32
	No correction	26	421 (146)	[208, 771]	
Net mean flow (ml/min)	Background correction	26	0 (7)	[−15, 13]	0.69
	No correction	26	0 (7)	[−18, 12]	

Table II. Mean value and standard deviation of CSF flow parameters measured at C2C3 and pontine cistern levels.

	C2C3		Pontine Cistern	
	Mean (SD)	Range [Min, Max]	Mean (SD)	Range [Min, Max]
n	26		16	
Mean stroke volume (μl/cycle)	383 (133)	[208, 772]	148 (75)	[43, 326]
Net mean flow (ml/min)	0 (7)	[−15, 13]	4 (5)	[−2, 15]
Peak maximum velocity (mm/s)	70 (20)	[38, 96]	32 (16)	[14, 71]
Peak minimum velocity (mm/s)	−52 (23)	[−89, −23]	−27 (17)	[−83, −11]
Area (mm^2)	93 (31)	[41, 157]	108 (42)	[28, 190]

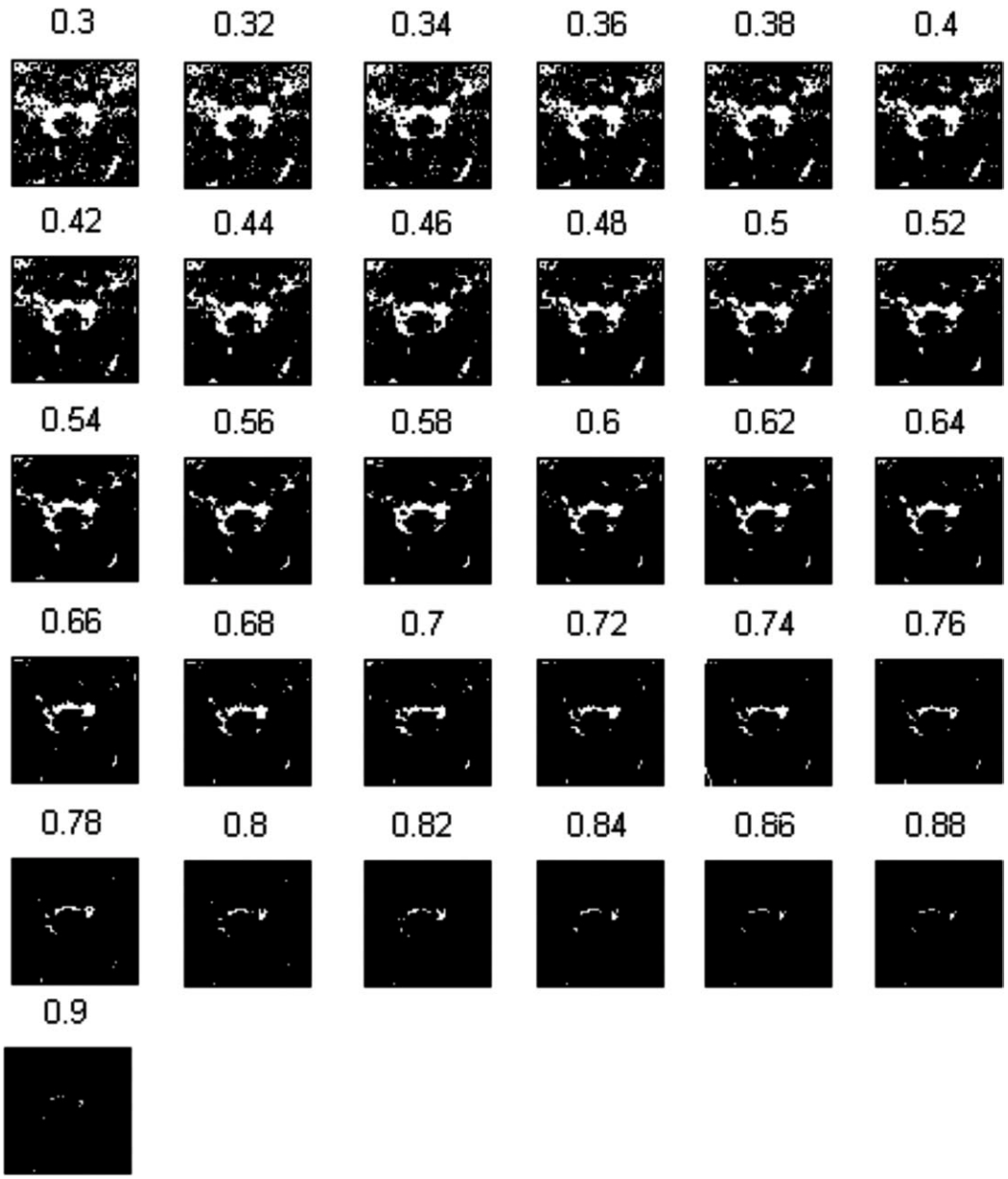

Figure 5. Threshold values (ranging from 0.3 to 0.9 in steps of 0.02) were applied to the correlation map to define the CSF region at the C2C3 level. Use of the threshold value suggested by Alperin (0.75), causes the segmented region to be underestimated. Using the threshold value calculated with our method (0.4), the number of pixels to cluster is not reduced and so the segmented region is not underestimated. The pixels containing flow were extracted as a function of the attributes given in the text and in the caption to Figure 6.

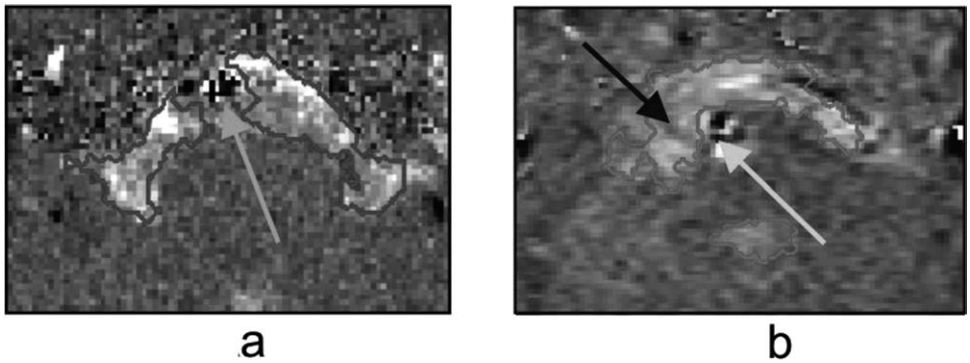

Figure 6. (a) The automatically segmented pontine cistern. (b) Observer intervention was needed to correctly segment the pontine cistern. The observer had to select the region to be analyzed (upper arrow) from two areas. The small region corresponds to CSF outflow through the fourth ventricle and the lower arrow indicates exclusion of the basilar artery from the segmented region.

using our present method was selected after comparison with anatomical images. Then, the number of pixels was not reduced and therefore the segmented region was not underestimated.

The distribution of pulsatility along the craniospinal axis plays an important role in the regulation of intracranial pressure (Alperin et al., 1996). Quantification of flow dynamics in the various CSF flow pathways will help identify markers of neurological and cerebrovascular disease. The pontine cistern is a large, anatomically complex structure that contains the basilar artery (Fig. 6) and is notably difficult to segment. By using the presented method in 16 subjects, it was possible to delineate the pontine cistern by removing the basilar artery pixels. In only five of these 16 subjects, it was necessary to manually remove the fourth ventricle's CSF flow, which was automatically selected as a single ROI encompassing the pontine cistern area (Fig. 6).

The velocity offset is only a small fraction of the CSF velocity and may also contain noise caused by brain motion (Enzmann and Pelc, 1992). In this study, the influence of the background baseline region selected at different locations was not appraised. Previous work (Lee et al., 2004) indicated that the baseline region (selected at midbrain or temporal lobe levels) had no significant effect on systolic peak velocities and mean aqueductal flows. In this study, the selected baseline region was always close to the ROI, to exclude cervical and intracranial vascular structures (such as the epidural veins and the basilar artery, respectively).

In our experiments, when the maximum expected flow velocity exceeded the value of parameter *V*enc, the velocity artefact known as aliasing occurred. This aliasing phenomenon was automatically detected and the pixel velocity corrected in seven measurements. By using this software correction, we have never had to repeat an acquisition.

The distribution of CSF flow pulsatility in several regions of the craniospinal axis has been analyzed from several standpoints, to better understand neurological diseases such as normal pressure hydrocephalus (NPH) (Henry-Feugeas et al., 2000). Transfer functions and spatiotemporal relationships have been calculated so as to characterize the coupling of vascular flow with cervical subarachnoid space and ventricular CSF flows (Alperin et al., 1996; Baledent et al., 2004; Wagshul et al., 2006). Nevertheless, the disease mechanisms are still poorly known. Surgical treatment of NPH carries a significant risk and the response to shunt surgery mainly depends on appropriate selection of the patients. Hyperdynamic aqueductal stroke volumes have been used as a diagnostic test for NPH; Bradley et al. (1996) suggested using this parameter to predict a positive response to treatment. However, the aqueductal stroke volume is not fully reliable or reproducible and also depends on the MRI acquisition and image processing techniques. Furthermore, Kahlon et al. (2007) found that aqueductal stroke volume is not useful for selecting patients with NPH symptoms for shunt surgery. Their results emphasized the need to identify more reproducible markers, such as pontine and C2C3 CSF flows.

In all three ROIs, systolic peak velocities were slightly higher than diastolic peak velocities. At the C2C3 level, the peak velocities were very close to or greater than the chosen V_{enc} parameter. This was not a disadvantage in our analysis because the aliased pixels were automatically detected and corrected. We believe that the V_{enc} values used in our protocol represented the best compromise between the signal-to-noise ratio and the possible velocity measurement range.

In conclusion, the new method presented here enables rapid, reproducible, quantitative analysis of CSF flow in regions with complex and inhomogeneous flow patterns, such as the intracranial pontine cistern and the cervical subarachnoid spaces. Better overall knowledge of CSF dynamics should help us understand CSF flow disturbances such as NPH.

ACKNOWLEDGMENTS

MRI operators at Amiens' University Hospital are gratefully acknowledged their technical contribution.

REFERENCES

N. Alperin, MR-intracranial compliance and pressure: A method for noninvasive measurement of important neurophysiologic parameters, Methods Enzymol 386 (2004), 323–349.

N. Alperin and S.H. Lee, PUBS: Pulsatility-based segmentation of lumens conducting non-steady flow, Magn Reson Med 49 (2003), 934–944.

N. Alperin, E.M. Vikingstad, B. Gomez-Anson, and D.N. Levin, Hemodynamically independent analysis of cerebrospinal fluid and brain motion observed with dynamic phase contrast MRI, Magn Reson Med 35 (1996), 741–754.

O. Baledent, L. Fin, L. Khuoy, K. Ambarki, A.C. Gauvin, C. Gondry-Jouet, and M.E. Meyer, Brain hydrodynamics study by phase-contrast magnetic resonance imaging and transcranial color doppler, J Magn Reson Imaging 24 (2006), 995–1004.

O. Baledent, C. Gondry-Jouet, M.E. Meyer, G. de Marco, D. Le Gars, M.C. Henry-Feugeas, and I. Idy-Peretti, Relationship between cerebrospinal fluid and blood dynamics in healthy volunteers and patients with communicating hydrocephalus, Invest Radiol 39 (2004), 45–55.

O. Baledent, M.C. Henry-Feugeas, and I. Idy-Peretti, Cerebrospinal fluid dynamics and relation with blood flow. A magnetic resonance study with semiautomated cerebrospinal fluid segmentation, Invest Radiol 36 (2001), 368–377.

R.A. Bhadelia, A.R. Bogdan, R.F. Kaplan, and S.M. Wolpert, Cerebrospinal fluid pulsation amplitude and its quantitative relationship to cerebral blood flow pulsations: A phase-contrast MR flow imaging study, Neuroradiology 39 (1997), 258–264.

R.A. Bhadelia, A.R. Bogdan, and S.M. Wolpert, Analysis of cerebrospinal fluid flow waveforms with gated phase- contrast MR velocity measurements, AJNR Am J Neuroradiol 16 (1995) 389–400.

F.M. Box, A. Spilt, M.A. Van Buchem, R.J. van der Geest, and J.H.C. Reiber, Automatic model-based contour detection and blood flow quantification in small vessels with velocity encoded magnetic resonance imaging, Invest Radiol 38 (2003), 567–577.

W.G. Bradley Jr, Magnetic resonance imaging in the evaluation of cerebrospinal fluid flow abnormalities, Magn Reson Q 8 (1992), 169–196.

W.G. Bradley, D. Scalzo, J. Queralt, W.N. Nitz, D.J. Atkinson, and P. Wong, Normal-pressure hydrocephalus: Evaluation with cerebrospinal fluid flow measurements at MR imaging, Radiology 198 (1996), 523–529.

M. Egnor, L. Zheng, A. Rosiello, F. Gutman, and R. Davis, A model of pulsations in communicating hydrocephalus, Pediatr Neurosurg 36 (2002), 281–303.

D.R. Enzmann and N.J. Pelc, Normal flow patterns of intracranial and spinal cerebrospinal fluid defined with phase-contrast cine MR imaging, Radiology 178 (1991), 467–474.

D.R. Enzmann and N.J. Pelc brain motion: Measurement with phase-contrast MR Imaging, Radiology 185 (1992), 653–660.

D.R. Enzmann and N.J. Pelc Cerebrospinal fluid flow measured by phase-contrast cine MR, AJNR Am J Neuroradiol 14 (1993), 1301–1307, discussion 1309–1310.

D. Greitz, Cerebrospinal fluid circulation and associated intracranial dynamics. A radiologic investigation using MR imaging and radionuclide cisternography, Acta Radiol Suppl 386 (1993), 1–23.

D. Greitz, A. Franck, and B. Nordell, On the pulsatile nature of intracranial and spinal CSF-circulation demonstrated by MR imaging. Acta Radiol 34 (1993), 321–328.

M.C. Henry-Feugeas, I. Idy-Peretti, O. Baledent, A. Poncelet-Didon, G. Zannoli, J. Bittoun, and E. Schouman-Claeys, Origin of subarachnoid cerebrospinal fluid pulsations: a phase-contrast MR analysis, Magn Reson Imaging 18 (2000), 387–395.

M.C. Henry-Feugeas, I. Idy-Peretti, B. Blanchet, D. Hassine, G. Zannoli, and E. Schouman-Claeys, Temporal and spatial assessment of normal cerebrospinal fluid dynamics with MR imaging, Magn Reson Imaging 11 (1993), 1107–1118.

B. Kahlon, M. Annertz, F. Stahlberg, and S. Rehncrona, Is aqueductal stroke volume, measured with cine phase-contrast magnetic resonance imaging scans useful in predicting outcome of shunt surgery in suspected normal pressure hydrocephalus? Neurosurgery 60 (2007), 124–129.

D.S. Kim, J.U. Choi, R. Huh, P.H. Yun, and D.I. Kim, Quantitative assessment of cerebrospinal fluid hydrodynamics using a phase-contrast cine MR image in hydrocephalus, Childs Nervous System 15 (1999), 461–477.

S. Kozerke, R. Botnar, S. Oyre, M.B. Scheidegger, E.M. Pedersen, and P. Boesiger, Automatic vessel segmentation using active contours in cine phase contrast flow measurements, J Magn Reson Imaging 10 (1999), 41–51.

J.H. Lee, H.K. Lee, J.K. Kim, H.J. Kim, J.K. Park, and C.G. Choi, CSF flow quantification of the cerebral aqueduct in normal volunteers using phase contrast cine MR imaging, Korean J Radiol 5 (2004), 81–86.

P.H. Luetmer, J. Huston, J.A. Friedman, G.R. Dixon, R.C. Petersen, C.R. Jack, R.L. McClelland, and M.J. Ebersold, Measurement of cerebrospinal fluid flow at the cerebral aqueduct by use of phase-contrast magnetic resonance imaging: technique validation and utility in diagnosing idiopathic normal pressure hydrocephalus. Neurosurgery 50 (2002), 534–543.

J.B. MacQueen, Some methods for classification and analysis of multivariate observations. 5-th Berkeley Symposium on Mathematical Statistics and Probability. Berkeley, University of California, 1967, pp. 281–297.

T. Miyati, M. Mase, T. Banno, T. Kasuga, K. Yamada, H. Fujita, K. Koshida, S. Sanada, and M. Onoguchi, Frequency analyses of CSF flow on cine MRI in normal pressure hydrocephalus. Eur Radiol 13 (2003), 1019–1024.

T. Miyati, M. Mase, H. Kasai, M. Hara, K. Yamada, Y. Shibamoto, M. Soellinger, C. Baltes, and R. Luechinger, Noninvasive MRI assessment of intracranial compliance in idiopathic normal pressure hydrocephalus, J Magn Reson Imaging 26 (2007), 274–278.

W.R. Nitz, W.G. Bradley, A.S. Watanabe, R.R. Lee, B. Burgoyne, R.M. Osullivan, and M.D. Herbst, Flow dynamics of cerebrospinal fluid: assessment with phase-contrast velocity MR imaging performed with retrospective cardiac gating, Radiology 183 (1992), 395–405.

N.J. Pelc, Flow quantification and analysis methods, Magn Reson Imaging Clin N Am 3 (1995), 413–424.

C. Thomsen, F. Stahlberg, M. Stubgaard, and B. Nordell, Fourier analysis of cerebrospinal fluid flow velocities: MR imaging study. The Scandinavian flow group, Radiology 177 (1990), 659–665.

M.E. Wagshul, J.J. Chen, M.R. Egnor, E.J. McCormack, and P.E. Roche, Amplitude and phase of cerebrospinal fluid pulsations: experimental studies and review of the literature, J Neurosurg 104 (2006), 810–819.

R.L. Wolf, R.L. Ehman, S.J. Riederer, and P.J. Rossman, Analysis of systematic and random error in MR volumetric flow measurements, Magn Reson Med 30 (1993), 82–91.

C. Yuan, E. Lin, J. Millard, and J.N. Hwang, Closed contour edge detection of blood vessel lumen and outer wall boundaries in black-blood MR images, Magn Reson Imaging 17 (1999), 257–266.